Inorg. Chem. **2008**, *47*, 957–968

Strong Intra- and Intermolecular Aurophilic Interactions in a New Series of Brilliantly Luminescent Dinuclear Cationic and Neutral Au(I) Benzimidazolethiolate Complexes

Jacob Schneider, Young-A Lee, Javier Pérez, William W. Brennessel, Christine Flaschenriem, and Richard Eisenberg*

Department of Chemistry, University of Rochester, Rochester, New York 14627

Received September 7, 2007

The structural and photophysical properties of a new series of cationic and neutral Au(I) dinuclear compounds (**1** and **2**, respectively) bridged by bis(diphenylphosphino)methane (dppm) and substituted benzimidazolethiolate (X–BIT) ligands, where X = H (**a**), Me (**b**), OMe (**c**), and Cl (**d**), have been studied. Monocationic complexes, $[Au_2(\mu\text{-X–BIT})(\mu\text{-dppm})](CF_3CO_2)$, were prepared by the reaction of $[Au_2(\mu\text{-dppm})](CF_3CO_2)_2$ with 1 equiv of X–BIT in excellent yields. The cations **1a**–**1d** possess similar molecular structures, each with a linear coordination geometry around the Au(I) nuclei, as well as relatively short intramolecular Au(I)···Au(I) separations ranging between 2.88907(6) Å for **1d** and 2.90607(16) Å for **1a** indicative of strong aurophilic interactions. The cations are violet luminescent in CH_2Cl_2 solution with a λ_{em}^{max} of ca. 365 nm, assigned as ligand-based or metal-centered (MC) transitions. Three of the cationic complexes, **1a**, **1b**, and **1d**, exhibit unusual *luminescence tribochromism* in the solid-state, in which the photoemission is shifted significantly to higher energy upon gentle grinding of microcrystalline samples with $\Delta E = 1130\ cm^{-1}$ for **1a**, $670\ cm^{-1}$ (**1b**), and $870\ cm^{-1}$ (**1d**). The neutral dinuclear complexes, $[Au_2(\mu\text{-X–BIT})(\mu\text{-dppm})]$ (**2a**–**2d**) were formed in good yields by the treatment of a CH_2Cl_2 solution of cationic compounds (**1**) with NEt_3. **2a**–**2d** aggregate to form dimers having substantial intra- and intermolecular aurophilic interactions with unsupported Au(I)···Au(I) intermolecular distances in the range of 2.8793(4)–2.9822(8) Å, compared with intramolecular bridge-supported separations of 2.8597(3)–2.9162(3) Å. **2a**-**2d** exhibit brilliant luminescence in the solid-state and in DMSO solution with red-shifted λ_{em}^{max} energies in the range of 485–545 nm that are dependent on X–BIT and assigned as ligand-to-metal–metal charge transfer (LMMCT) states based in part on the extended Au···Au···Au···Au interactions.

Introduction

In recent years, there has been a developing interest in luminescent metal complexes because of their possible application as dopant emitters in organic light emitting device technology.[1,2] In this context, Au(I) complexes represent potential targets of opportunity, owing to their intense, long-lived luminescence in the solid-state with a wide range of emission energies.[3–5] The tendency of Au(I) complexes to aggregate through closed-shell "aurophilic" interactions[6–8] plays a key role in their luminescence properties and in determining their consequent solid-state structures.[9–13] Additionally, these types of closed-shell aggregates may also be influenced by hydrogen-bonding interactions between Au(I) complexes.[11,14–17] A number of different emitting states have been proposed for Au(I) complexes including metal-

* To whom correspondence should be addressed. Email: eisenberg@chem.rochester.edu.

(1) Holder, E.; Langeveld, B. M. W.; Schubert, U. S. *Adv. Mater. (Weinheim, Germany)* **2005**, *17* (9), 1109−1121.
(2) Evans, R. C.; Douglas, P.; Winscom, C. J. *Coord. Chem. Rev.* **2006**, *250 (15+16)*, 2093−2126.
(3) Ramamurthy, V.; Schanze, K. S. *Mol. Supramol. Photochem.* **1999**, *4*, 345.
(4) Wang, Q.-M.; Lee, Y.-A.; Crespo, O.; Deaton, J.; Tang, C.; Gysling, H. J.; Gimeno, M. C.; Larraz, C.; Villacampa, M. D.; Laguna, A.; Eisenberg, R. *J. Am. Chem. Soc.* **2004**, *126* (31), 9488−9489.
(5) Ma, Y.; Zhou, X.; Shen, J.; Chao, H.-Y.; Che, C.-M. *Appl. Phys. Lett.* **1999**, *74* (10), 1361−1363.
(6) Schmidbaur, H.; Graf, W.; Müller, G. *Angew. Chem., Int. Ed. Engl.* **1988**, *27* (3), 417−419.
(7) Scherbaum, F.; Huber, B.; Müller, G.; Schmidbaur, H. *Angew. Chem., Int. Ed. Engl.* **1988**, *27* (11), 1542−1544.
(8) Scherbaum, F.; Grohmann, A.; Huber, B.; Krüger, C.; Schmidbaur, H. *Angew. Chem., Int. Ed. Engl.* **1988**, *27* (11), 1544−1546.

10.1021/ic701763x CCC: $40.75
Published on Web 01/11/2008

Scheme 1

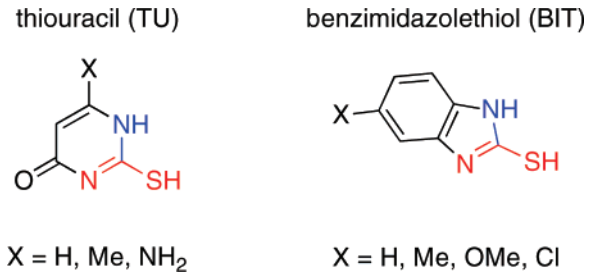

centered or cluster-based (MC), ligand-to-metal charge transfer (LMCT), ligand-to-metal−metal charge transfer (LMMCT), and intraligand (IL), and often a combination of two or more of them has been assigned to explain the observed luminescence behavior.[12,18−27]

The present study describes the structural and photophysical properties of new dinuclear cationic and neutral Au(I) complexes bridged by bis(diphenylphosphino)methane (dppm) and a series of benzimidazolethiolate ligands (X−BIT) (Scheme 1). The study of these systems was undertaken because an unusual behavior, termed luminescence tribochromism, and was seen in a closely related set of complexes in which the bridging N, S ligand was a derivative of thiouracil (X−TU). In luminescence tribochromism, a change in photoemission energy (as well as intensity) occurs in solid-state samples upon the application of mild pressure. For the X−TU complexes reported earlier, a bright cyan photoemission was turned on upon the gentle crushing of colorless, nonemissive crystals of the complexes.[28] In the present study, three of the cationic complexes exhibit luminescence tribochromism, but the behavior differs from that reported earlier. From the structural characterization of the new complexes, we are able to assess the extent and magnitude of aurophilic interactions in these complexes and compare them with those found in the previously reported systems. Like the X−TU complexes, the cationic X−BIT complexes **1** exhibit significant intramolecular Au···Au interactions but significantly different intermolecular contacts, whereas the neutral complexes **2** show evidence of strong inter- as well as intramolecular Au···Au interactions, as was seen for the corresponding X−TU systems.[28]

Experimental Section

Characterization and Instrumentation. All of the NMR spectra were recorded on either Bruker Avance 400 or 500 MHz spectrometers. ^{1}H NMR chemical shifts (in ppm) are relative to $SiMe_4$ and referenced using the chemical shift of DMSO-d_6. ^{31}P NMR chemical shifts (in ppm) are relative to an external 85% solution of H_3PO_4 in the appropriate solvent. For cationic complexes, mass determinations were carried out by electrospray ionization mass spectrometry (ESI-MS) using a Hewlett-Packard Series 1100 mass spectrometer (Model A) equipped with a quadrupole mass filter. For neutral complexes, mass spectra were measured using a Hewlett-Packard 1100 series mass selective detector operated with an electrospray source and the detection of positive and negative ions. The samples were dissolved in CH_2Cl_2 for **1a**−**1d** or CH_2Cl_2/CH_3OH (1:1 v/v) for **2a**−**2d** and pumped into the spray chamber using 100% CH_3OH. Absorption spectra were recorded using a Hitachi U2000 scanning spectrophotometer (200−1100 nm). Steady-state emission spectra were obtained using a Spex Fluoromax-P fluorimeter corrected for instrument response with monochromators positioned with a 2 nm band-pass. The free X−BIT ligand concentration of solution samples was 1.0×10^{-5} M in CH_2Cl_2/MeOH (1:1, v/v) and each sample was degassed by at least two freeze−pump−thaw cycles. The metal complex concentration of solution samples was 1.0×10^{-5} M in CH_2Cl_2 for cationic complexes or DMSO for neutral complexes, and each sample was degassed by at least three freeze−pump−thaw cycles. Solid-state emission samples were prepared as a 10% (w/w) mixture of the complex in a matrix of finely ground KBr. Elemental analyses were performed by Quantitative Technologies Inc..

Crystallographic Structure Determinations. Crystals were attached to glass fibers and mounted under a stream of N_2, maintained at either 100.0(1) K or 193(2) K for **1b**, on a Bruker *SMART* platform diffractometer equipped with an APEX II CCD detector, positioned at −33° in 2θ and 5.0 cm from the samples. The X-ray source, powered at 50 kV and 30 mA, provided Mo Kα radiation (λ = 0.71073 Å, graphite monochromator). Preliminary random samplings of reflections were used to determine unit cells and orientation matrices.[29] Complete data collections were obtained by ω scans of 183° (0.5° steps) at four different φ settings. Final cell constants were calculated from the xyz centroids of approximately 4000 strong reflections from the actual data collection after integration.[30] The data were additionally scaled and corrected for absorption.[31] Space groups were determined based on systematic

(9) King, C.; Wang, J.-C.; Khan, M. N. I.; Fackler, J. P., Jr. *Inorg. Chem.* **1989**, *28* (11), 2145−2149.
(10) Forward, J. M.; Fackler, J. P., Jr.; Assefa, Z. *Optoelectronic Properties of Inorganic Compounds*, Roundhill, D. M., Fackler, J. P., Jr., Eds.; Plenum Press: New York, 1999; pp 195−229.
(11) Hao, L.; Mansour, M. A.; Lachicotte, R. J.; Gysling, H. J.; Eisenberg, R. *Inorg. Chem.* **2000**, *39*, 5520−5529.
(12) Lee, Y.-A.; McGarrah, J. E.; Lachicotte, R. J.; Eisenberg, R. *J. Am. Chem. Soc.* **2002**, *124*, 10662−10663.
(13) White-Morris, R. L.; Stender, M.; Tinti, D. S.; Balch, A. L.; Rios, D.; Attar, S. *Inorg. Chem.* **2003**, *42* (10), 3237−3244.
(14) Tzeng, B.-C.; Schier, A.; Schmidbaur, H. Crystal Engineering of Gold(I) Thiolate Based Compounds via Cooperative Aurophilic and Hydrogen-Bonding Interactions. *Inorg. Chem.* **1999**, *38*, 3978−3984.
(15) Hao, L.; Lachicotte, R. J.; Gysling, H. J.; Eisenberg, R. *Inorg. Chem.* **1999**, *99* (21), 4616−4617.
(16) Hunks, W. J.; Jennings, M. E.; Puddephatt, R. J. *Inorg. Chem.* **2002**, *41*, 4590−4598.
(17) Wilton-Ely, J. D. E. T.; Schier, A.; Mitzel, N. W.; Nogai, S.; Schmidbaur, H. *J. Organomet. Chem.* **2002**, *643*−*644*, 313−323.
(18) Tzeng, B.-C.; Liao, J.-H.; Lee, G.-H.; Peng, S.-M. *Inorg. Chim. Acta* **2004**, *357* (5), 1405−1410.
(19) Tzeng, B.-C.; Chan, C.-K.; Cheung, K.-K.; Che, C.-M.; Peng, S.-M. *Chem. Commun.* **1997**, 135−136.
(20) Li, D.; Che, C.-M.; Peng, S.-M.; Liu, S.-T.; Zhou, Z.-Y.; Mak, T. C. W. *J. Chem. Soc., Dalton Trans.* **1993**, 189−194.
(21) Bardají, M.; Calhorda, M. J.; Costa, P. J.; Jones, P. G.; Laguna, A.; Pérez, M. R.; Villacampa, M. D. *Inorg. Chem.* **2006**, *45* (3), 1059−1068.
(22) Forward, J. M.; Boohmann, D.; Fackler, J. P.; Staples, R. J. *Inorg. Chem.* **1995**, *34*, 6330−6336.
(23) Yam, V. W. W.; Chan, C.-L.; Li, C.-K.; Wong, K. M.-C. Molecular *Coord. Chem. Rev.* **2001**, *216*−*217*, 173−194.
(24) Ho, S. Y.; Cheng, E. C.-C.; Tiekink, E. R. T.; Yam, V. W.-W. *Inorg. Chem.* **2006**, *45 (20)*, 8165−8174.
(25) Chen, J.; Mohamed, A. A.; Abdou, H. E.; Bauer, J. A. K.; Fackler, J. P., Jr.; Bruce, A. E.; Bruce, M. R. M. *Chem. Commun.* **2005**, *(12)*, 1575−1577.
(26) Tzeng, B.-C.; Yeh, H.-T.; Huang, Y.-C.; Chao, H.-Y.; Lee, G.-H.; Peng, S.-M. *Inorg. Chem.* **2003**, *42 (19)*, 6008−6014.
(27) Yam, V. W. W.; Cheng, E. C. C.; Cheung, K. K. *Angew. Chem., Int. Ed.* **1999**, *38* (1−2), 197−199.
(28) Lee, Y.-A.; Eisenberg, R. *J. Am. Chem. Soc.* **2003**, *125*, 7778−7779.
(29) *APEX2 V2.1*−*0*, Bruker AXS: Madison, WI, 2006.
(30) *SAINT V7.34A*, Bruker AXS: Madison, WI, 2006.

absences, intensity statistics, and space group frequencies. Structures were solved by direct or Patterson methods.[32,33] Non-hydrogen atoms were located by difference Fourier syntheses, and their positions were refined with anisotropic displacement parameters by full-matrix least-squares cycles on F^2.[33] All of the hydrogen atoms, unless otherwise noted, were placed geometrically and refined as riding atoms with relative isotropic displacement parameters. For **1b**, **1d**, and **2d**, reflection contributions from highly disordered solvent molecules that include dichloromethane, diethyl ether, or both, could not be modeled and were removed using the program *PLATON*, function *SQUEEZE*.[34,35] The final set of refinement cycles, run to convergence, provided the reported quality assessment parameters.

Materials. Potassium tetrachloroaurate(III) (Aldrich), silver trifluoroacetate (Aldrich), bis(diphenylphosphino)methane (dppm) (Strem), 2-mercaptobenzimidazole (H−BIT) (Aldrich), 2-mercapto-5-methylbenzimidazole (Me−BIT) (Aldrich), 5-methoxy-2-benzimidazolethiol (OMe−BIT) (Aldrich), 5-chlorobenzimidazole-2-thiol (Cl−BIT) (Avocado), and DMSO-d_6 (Cambridge Isotope Laboratories) were purchased commercially and used without further purification. [Au_2(μ-dppm)Cl_2] was prepared according to the literature procedure.[5,36] All of the other solvents and reagents were purchased commercially and used without further purification.

Synthesis and Characterization of New Au(I) Complexes. [Au_2(μ-H−BIT)(μ-dppm)](CF_3CO_2) (1a). To a solution of [Au_2-(μ-dppm)Cl_2] (0.30 g, 0.353 mmol) in CH_2Cl_2 (15 mL) was added $AgCF_3CO_2$ (0.156 g, 0.706 mmol), and the white mixture was stirred at room temperature (RT) for 30 min while covered in foil. The suspension was filtered through a pad of celite, to remove the AgCl precipitate, and into a suspension of H−BIT (53 mg, 0.353 mmol) in CH_2Cl_2 (15 mL). The reaction mixture was stirred overnight at RT. The resulting solution was concentrated to ∼5 mL, and the addition of Et_2O (75 mL) gave an off-white precipitate. The precipitate was collected by filtration and washed with Et_2O. Recrystallization by slow diffusion of Et_2O into a CH_2Cl_2 solution gave a white colored product. Yield 71%. Mp 215 °C (dec). ESMS (*m*/*z*): 927.0, [M-(CF_3CO_2)]. ^{1}H NMR (DMSO-d_6, 400 MHz): δ 13.61 (br s, 1H, N-*H*), 7.91−7.72 (m, 9H, dppm phenyl and H−BIT aryl), 7.54−7.35 (br m, 13H, dppm phenyl and H−BIT aryl), 7.35−7.24 (m, 2H, H−BIT aryl), 4.92 (t, J_{HP} = 13.7 Hz, 2H, dppm). ^{31}P{^{1}H} NMR (DMSO-d_6, 162 MHz): δ 33.7 (d, J_{PP} = 51 Hz), 28.0 (d, J_{PP} = 51 Hz). Anal. Calcd for $C_{34}H_{27}$-$Au_2F_3N_2O_2P_2S$: C, 39.24; H, 2.62; N, 2.69. Found: C, 39.63; H, 2.65; N, 2.71.

[Au_2(μ-Me−BIT)(μ-dppm)](CF_3CO_2) (1b). This compound was prepared by the same method as for **1a**, using Me−BIT (58 mg, 0.353 mmol) in place of H−BIT. Recrystallization by slow diffusion of Et_2O into a CH_2Cl_2 solution of the complex gave a white colored product. Yield 73%. Mp 199 °C (dec). ESMS (*m*/*z*): 941.0, [M-(CF_3CO_2)]. ^{1}H NMR (DMSO-d_6, 400 MHz): δ 13.48 (br s, 1H, N-*H*), 7.91−7.71 (m, 8H, dppm phenyl), 7.68 (d, J_{HH} = 8.2 Hz, 1/2H, Me−BIT aryl), 7.61 (s, 1/2H, Me−BIT aryl), 7.55−7.35 (br m, 12H, dppm phenyl), 7.33 (d, J_{HH} = 8.1 Hz, 1/2H, Me−BIT aryl), 7.25 (s, 1/2H, Me−BIT aryl), 7.10 (br t, 1H, Me−BIT aryl), 4.92 (t, J_{HP} = 13.7 Hz, 2H, dppm), 2.42 (s, 3H, *Me*-BIT). ^{31}P{^{1}H} NMR (DMSO-d_6, 162 MHz): δ 33.6 (d, J_{PP} = 51 Hz), 27.9 (d, J_{PP} = 51 Hz), 27.8 (d, J_{PP} = 52 Hz). Anal. Calcd for $C_{35}H_{29}$-$Au_2F_3N_2O_2P_2S$: C, 39.86; H, 2.77; N, 2.66. Found: C, 39.58; H, 2.82; N, 2.60.

[Au_2(μ-OMe−BIT)(μ-dppm)](CF_3CO_2) (1c). This compound was prepared by the same method as for **1a**, using OMe−BIT (63 mg, 0.353 mmol) in place of H−BIT. Recrystallization by slow diffusion of Et_2O or hexane into a CH_2Cl_2 solution of the complex gave a white colored product. Yield 78%. Mp 206 °C (dec). ESMS (*m*/*z*): 957.0, [M-(CF_3CO_2)]. ^{1}H NMR (DMSO-d_6, 400 MHz): δ 13.45 (br s, 1H, N-*H*), 7.92−7.71 (m, 8H, dppm phenyl), 7.70 (d, J_{HH} = 8.8 Hz, 1/2H, OMe−BIT aryl), 7.51−7.37 (br m, 12H, dppm phenyl), 7.34 (d, J_{HH} = 8.8 Hz, 1/2H, OMe−BIT aryl), 7.30 (s, 1/2H, OMe−BIT aryl), 6.93 (br s, 1H, OMe−BIT aryl), 6.88 (d, J_{HH} = 8.8 Hz, 1/2H, OMe−BIT aryl), 4.91 (t, J_{HP} = 13.7 Hz, 2H, dppm), 3.80 (s, 3H, O*Me*-BIT). ^{31}P{^{1}H} NMR (DMSO-d_6, 162 MHz): δ 33.7 (d, J_{PP} = 52 Hz), 33.6 (d, J_{PP} = 51 Hz), 28.1 (d, J_{PP} = 51 Hz), 27.8 (d, J_{PP} = 51 Hz). Anal. Calcd for $C_{35}H_{29}$-$Au_2F_3N_2O_3P_2S$: C, 39.26; H, 2.73; N, 2.62. Found: C, 39.77; H, 2.60; N, 2.34.

[Au_2(μ-Cl−BIT)(μ-dppm)](CF_3CO_2) (1d). This compound was prepared by the same method as for **1a**, using Cl−BIT (65 mg, 0.353 mmol) in place of H−BIT. Recrystallization by slow diffusion of Et_2O into a CH_2Cl_2 solution of the complex gave a pale yellow colored product. Yield 70%. Mp 188 °C (dec). ESMS (*m*/*z*): 961.0, [M-(CF_3CO_2)]. ^{1}H NMR (DMSO-d_6, 500 MHz): δ 13.79 (br s, 1H, N-*H*), 8.01 (s, 1/2H, Cl−BIT aryl), 7.95−7.70 (m, 8 1/2 H, dppm phenyl and Cl−BIT aryl), 7.59−7.32 (br m, 13H, dppm phenyl and Cl−BIT aryl), 7.31 (br t, 1H, Cl−BIT aryl), 4.99−4.82 (m, 2H, dppm). ^{31}P{^{1}H} NMR (DMSO-d_6, 202 MHz): δ 33.1 (br d, J_{PP} = 52 Hz), 27.1 (br t). Anal. Calcd for $C_{34}H_{26}Au_2$-$ClF_3N_2O_2P_2S$: C, 37.99; H, 2.44; N, 2.61. Found: C, 37.77; H, 2.25; N, 2.28.

[Au_2(μ-H−BIT)(μ-dppm)] (2a). To a solution of **1a** (75 mg, 0.072 mmol) in CH_2Cl_2 (20 mL) was added NEt_3 dropwise until a bright green suspension began to form. After stirring overnight at RT, the light green suspension was collected by filtration, washing with H_2O (3 × 5 mL), cold MeOH (3 × 5 mL) and Et_2O. Yield 76%. Mp > 250 °C. ESMS (*m*/*z*): 926.8, [M]. ^{1}H NMR (DMSO-d_6, 500 MHz): δ 7.92−7.70 (m, 8H, dppm phenyl), 7.58−7.31 (br m, 13H, dppm phenyl and H−BIT aryl), 7.24 (d, J_{HH} = 7.7 Hz, 1H, H−BIT aryl), 6.89−6.81 (m, 2H, H−BIT aryl), 4.78 (t, J_{HP} = 13.3 Hz, 2H, dppm). ^{31}P{^{1}H} NMR (DMSO-d_6, 202 MHz): δ 33.6 (d, J_{PP} = 56 Hz), 28.1 (d, J_{PP} = 56 Hz). Anal. Calcd for $C_{32}H_{26}Au_2N_2P_2S$: C, 41.48; H, 2.83; N, 3.02. Found: C, 40.68; H, 2.63; N, 2.86.

[Au_2(μ-Me−BIT)(μ-dppm)] (2b). The method to prepare this compound was analogous to that for **2a** beginning with **1b** (75 mg, 0.071 mmol). Yield 73%. Mp > 250 °C. ESMS (*m*/*z*): 940.8, [M]. ^{1}H NMR (DMSO-d_6, 400 MHz): δ 7.88−7.70 (m, 8H, dppm phenyl), 7.51−7.33 (br m, 12H, dppm phenyl), 7.32 (d, J_{HH} = 7.7 Hz, 1/2H, Me−BIT aryl), 7.24 (s, 1/2H, Me−BIT aryl), 7.11 (d, J_{HH} = 7.8 Hz, 1/2H, Me−BIT aryl), 7.04 (s, 1/2H, Me−BIT aryl), 6.67 (br t, 1H, Me−BIT aryl), 4.76 (t, J_{HP} = 13.4 Hz, 2H, dppm), 2.32 (s, 3H, *Me*-BIT). ^{31}P{^{1}H} NMR (DMSO-d_6, 162 MHz): δ 34.1 (d, J_{PP} = 56 Hz), 28.6 (d, J_{PP} = 56 Hz), 28.5 (d, J_{PP} = 56 Hz). Anal. Calcd for $C_{33}H_{28}Au_2N_2P_2S$: C, 42.14; H, 3.00; N, 2.98. Found: C, 41.57; H, 3.00; N, 3.03.

[Au_2(μ-OMe−BIT)(μ-dppm)] (2c). The method to prepare this compound was analogous to that for **2a** beginning with **1c** (75 mg, 0.071 mmol). Yield 70%. Mp > 250 °C. ESMS (*m*/*z*): 956.9, [M].

(31) Sheldrick, G. M. *SADABS V2004/1*, University of Göttingen: Göttingen, Germany, 2004.
(32) Altomare, A.; Burla, M. C.; Camalli, M.; Cascarano, G. L.; Giacovazzo, C.; Guagliardi, A.; Moliterni, A. G. G.; Polidori, G.; Spagna, R. *SIR97: A New Program for Solving and Refining Crystal Structures*; Istituto di Cristallografia, CNR: Bari, Italy, 1999.
(33) *SHELXTL V6.14*, Bruker AXS: Madison, WI, 2000.
(34) Spek, A. L. *PLATON V300106*, Utrecht University: Utrecht, The Netherlands, 2006.
(35) Spek, A. L. *J. Appl. Crystallogr.* **2003**, *36*, 7−13.
(36) Schmidbaur, H.; Wohlleben, A.; Wagner, F.; Orama, O.; Huttner, G. *Chem. Ber.* **1977**, *110*, 1748−1754.

Scheme 2

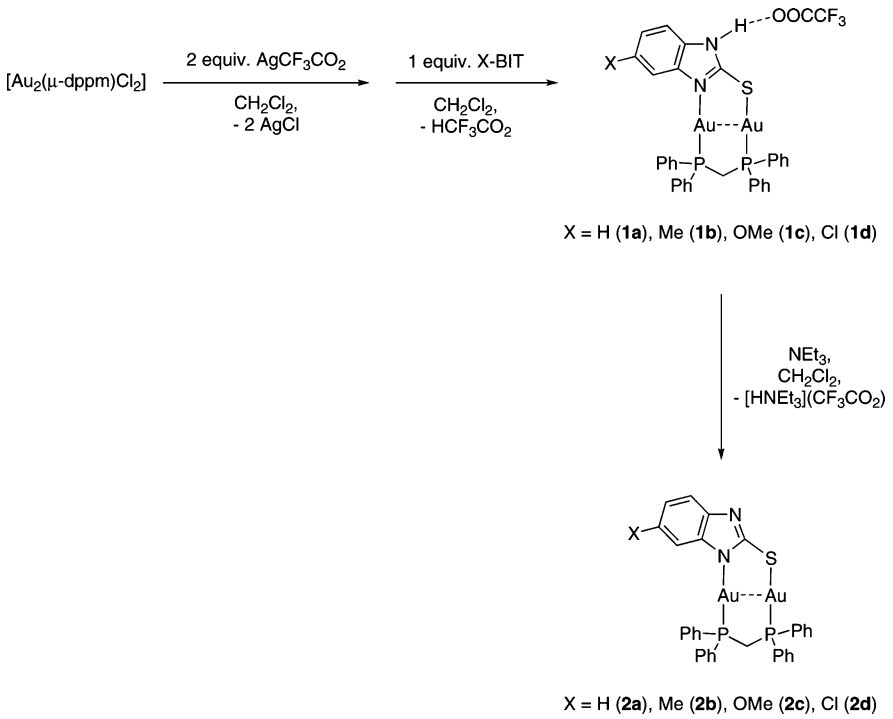

^{1}H NMR (DMSO-d_6, 400 MHz): δ 7.90−7.69 (m, 8H, dppm phenyl), 7.50−7.33 (br m, 12H, dppm phenyl), 7.32 (d, J_{HH} = 7.1 Hz, 1/2H, OMe−BIT aryl), 7.12 (d, J_{HH} = 7.4 Hz, 1/2H, OMe−BIT aryl), 7.00 (s, 1/2H, OMe−BIT aryl), 6.81 (s, 1/2H, OMe−BIT aryl), 6.50 (br m, 1H, OMe−BIT aryl), 4.77 (t, J_{HP} = 13.3 Hz, 2H, dppm), 3.71 (s, 3H, O*Me*-BIT). ^{31}P{^{1}H} NMR (DMSO-d_6, 162 MHz): δ 34.2 (d, J_{PP} = 58 Hz), 34.1 (d, J_{PP} = 56 Hz), 28.7 (d, J_{PP} = 56 Hz), 28.6 (d, J_{PP} = 55 Hz). Anal. Calcd for $C_{33}H_{28}Au_2N_2OP_2S$: C, 41.43; H, 2.95; N, 2.93. Found: C, 40.65; H, 2.78; N, 2.82.

[Au$_2$(μ-Cl−BIT)(μ-dppm)] (2d). The method to prepare this compound was analogous to that for **2a** beginning with **1d** (75 mg, 0.071 mmol). Yield 78%. Mp > 250 °C. ESMS (*m*/*z*): 960.9, [M]. ^{1}H NMR (DMSO-d_6, 400 MHz): δ 7.90−7.70 (m, 8H, dppm phenyl), 7.52−7.33 (br m, 13H, dppm phenyl and Cl−BIT aryl), 7.23 (br s, 1/2H, Cl−BIT aryl), 7.20 (s, 1/2H, Cl−BIT aryl), 6.84 (br t, 1H, Cl−BIT aryl), 4.80−4.72 (m, 2H, dppm). ^{31}P{^{1}H} NMR (DMSO-d_6, 162 MHz): δ 34.2 (d, J_{PP} = 55 Hz), 34.1 (d, J_{PP} = 56 Hz), 28.6 (d, J_{PP} = 55 Hz), 28.4 (d, J_{PP} = 55 Hz). Anal. Calcd for $C_{32}H_{25}Au_2ClN_2P_2S$: C, 39.99; H, 2.62; N, 2.92. Found: C, 39.82; H, 2.32; N, 2.92.

Results and Discussion

Synthesis and Characterization. The monocationic complexes, [Au$_2$(μ-X−BIT)(μ-dppm)](CF$_3$CO$_2$), were prepared for X = H (**1a**), Me (**1b**), OMe (**1c**), and Cl (**1d**), by the reaction of [Au$_2$(μ-dppm)](CF$_3$CO$_2$)$_2$, generated in situ from the reaction of [Au$_2$(μ-dppm)Cl$_2$] with 2 equiv of AgCF$_3$CO$_2$, with 1 equiv of X−BIT in excellent yields (Scheme 2). **1a**−**1d** were characterized by both ^{1}H and ^{31}P{^{1}H} NMR spectroscopies, mass spectrometry, elemental analyses, and single-crystal X-ray diffraction. The ^{1}H NMR data of **1b**−**1d** reveal the presence of two geometric isomers, described as *m*- and *p*-isomers in Scheme 3, in a 1:1 ratio that forms upon the reaction of the in situ-generated [Au$_2$(μ-dppm)](CF$_3$CO$_2$)$_2$ with 1 equiv of X−BIT for X = Me, OMe, and Cl, giving six rather than three aromatic resonances, some of which overlap with one another, that correspond to the substituted BIT ligand, plus a broad resonance from the uncoordinated N−H imidazole proton at ca. 13.5 ppm. As an example, the ^{1}H NMR spectra of **1a** and **1c** are shown in Figure 1.

Scheme 3

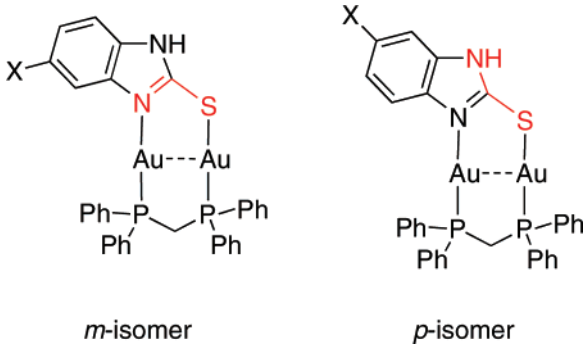

The ^{31}P{^{1}H} NMR data are also of interest for cationic complexes **1a**−**1d**. Whereas **1a** shows two doublets (J_{PP} = 51 Hz) that correspond to the two inequivalent phosphorus nuclei, in which one Au−P is trans to the benzimidazole nitrogen atom and the other Au−P is trans to the thiolate, complexes **1b**−**1d** each exhibit two sets of doublets corresponding to the two isomers present in a 1:1 ratio with the same J_{PP} of 51−52 Hz. Figure 2 illustrates the spectra of **1a** and **1c**, with two doublets observed for **1a** and two sets of doublets observed for **1c**. Upon heating **1b**−**1d** to 60 °C in DMSO-d_6, no coalescence is observed, indicating that rapid interconversion between the *m*- and *p*-isomers that would involve Au−N bond cleavage and free rotation about the C−S bond of the BIT ligand does not occur on the NMR time scale. This observation contrasts with that observed for

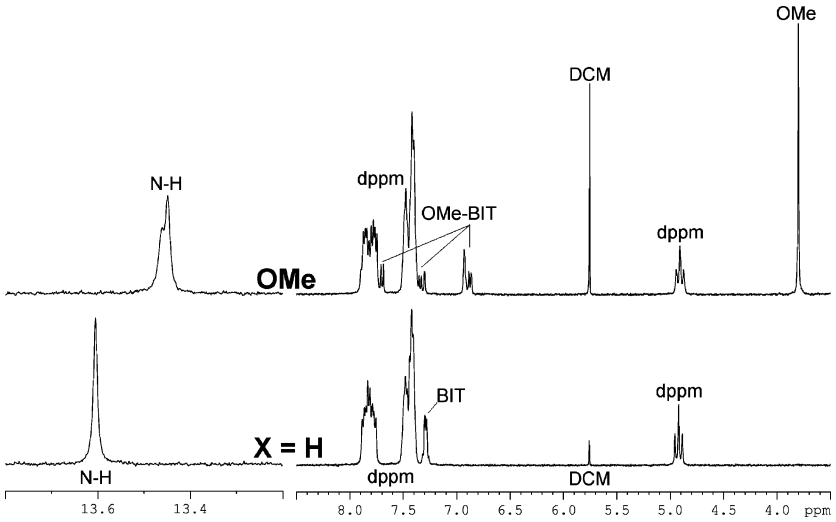

Figure 1. ^{1}H NMR spectra of **1a** (bottom) and **1c** (top) in DMSO-d_6. Notice the isomers that have formed in **1c** for both the OMe−BIT aryl resonances and also the N−H imidazole proton; DCM = dichloromethane.

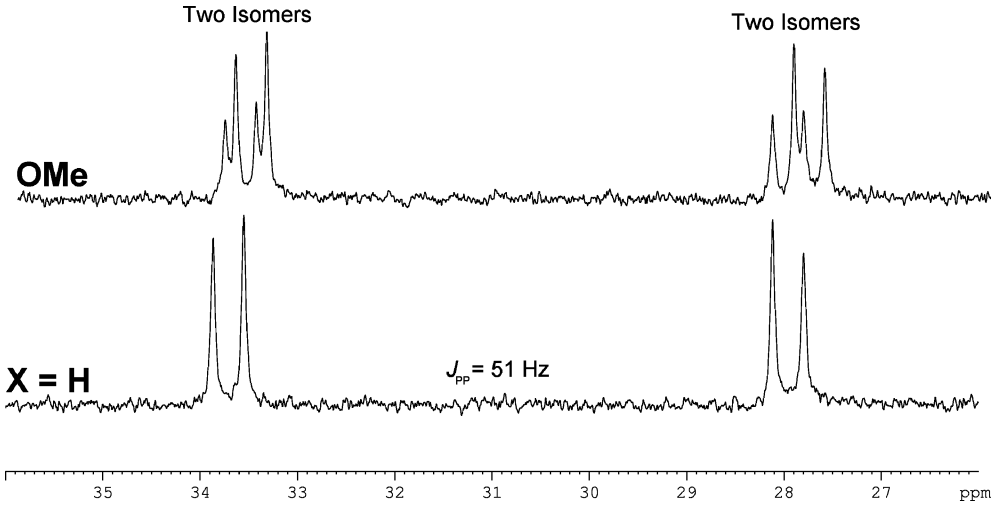

Figure 2. ^{31}P{^{1}H} NMR spectra of **1a** (bottom) and **1c** (top) in DMSO-d_6. Notice the two isomers that have formed in **1c**.

a similar system, [Au(4,6-Me_2pym-2-S]$_2$, in which coalescence in the ^{1}H NMR spectrum was seen at only 30 °C, via the mechanism proposed to involve Au−N bond cleavage.[15]

Dissolution of the monocationic complexes, **1a**−**1d**, in CH_2Cl_2 followed by the slow addition of NEt_3 leads to the formation of a bright yellow-green precipitate corresponding to [Au_2(μ-X−BIT)(μ-dppm)], with X = H, Me, OMe, and Cl, for **2a**−**2d**, respectively, in good yields (Scheme 2). Similar spectroscopic behavior is observed for each of these complexes. Like **1b**−**1d**, the ^{1}H NMR data of **2b**−**2d** exhibit two sets of aromatic resonances, some overlapping, resulting from the substituted BIT ligand, as seen in Figure 3 for **2b** and **2d**. The one notable difference between the ^{1}H NMR spectra of the cationic and neutral complexes is the absence of the N−H resonance in the neutral complexes that is the result of deprotonation of the cationic complexes by NEt_3. A similar pattern exists for the ^{31}P{^{1}H} NMR spectra of the neutral complexes to that seen for the respective cationic systems **1a**−**1d**. Specifically, two doublets are seen for **2a**, and two sets of doublets are found for **2b**−**2d** with monosubstituted BIT ligands. An example is shown for **2c** and **2d** in Figure 4. Upon deprotonation of the cationic complexes (**1**) to give the neutral complexes (**2**), a change in J_{PP} is observed, from 51−52 Hz in the former to a slightly larger J_{PP} of 55−58 Hz in the latter.

Crystal Structure Determinations. Crystals of **1a**−**1d**, suitable for single-crystal X-ray diffraction, were grown by slow diffusion and/or layering of a nonpolar solvent such as diethylether or hexane into a dichloromethane solution containing the cationic complex as the trifluoroacetate salt. The unit cell, data collection and refinement parameters are summarized for **1a**−**1d** in Table 1 with selected bond lengths and angles given in Table 2. Structurally, **1a**−**1d** are very similar, with a linear coordination geometry at each Au(I) ion, and a close intramolecular Au···Au separation ranging from 2.8807(6) to 2.90607(16) Å (Table 2). The intramolecular Au···Au distances found for **1a**−**1d** are comparable to those found in analogous Au(I) complexes reported previously for N,S-bridged Au_2 systems: 2.8797(4) Å in [Au_2(μ-TU)(μ-dppm)](CF_3CO_2), and 2.8617(7) and 2.8864(6) Å in [Au_2(μ-Me−TU)(μ-dppm)](CF_3CO_2).[28] In comparison with the dinuclear N,S-bridged complex, [Au_2(μ-$SC_4H_2N_2O_2$)(μ-dppe)] where dppe = bis(diphenylphoshino)-ethane, the intramolecular Au···Au distances for **1a**−**1d** are

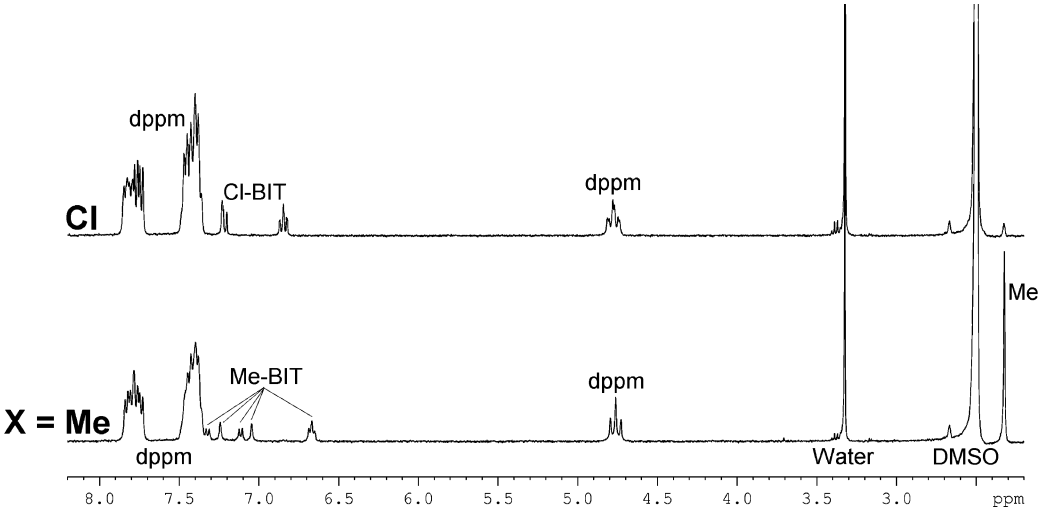

Figure 3. ^{1}H NMR spectra of **2b** (bottom) and **2d** (top) in DMSO-d_6; both show isomers, whereas the X−BIT aryl resonances for **2d** overlap, and those of **2b** do not.

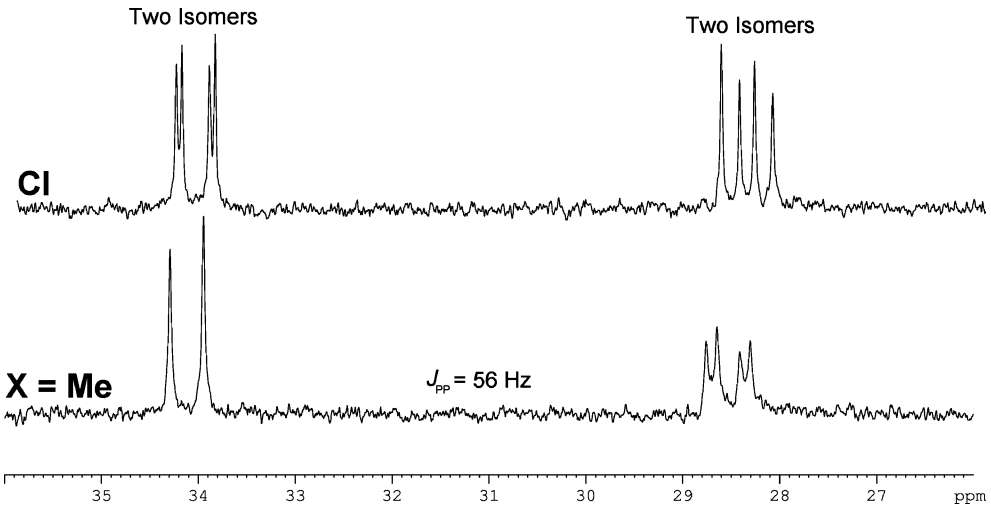

Figure 4. ^{31}P{^{1}H} NMR spectra of **2b** (bottom) and **2d** (top) in DMSO-d_6. Contrary to their respective ^{1}H NMR spectra, the isomeric resonances in **2b** are overlapping (doublet on the left), whereas those of **2d** are not.

slightly shorter than in the former complex, 2.9536(5) Å, which is not unexpected when increasing the bite angle of the bridging phosphine from dppm to dppe.[16]

Whereas the intramolecular Au···Au separations for **1a**−**1d** indicate strong aurophilic interactions, there are no significant intermolecular Au···Au interactions. This stands in sharp contrast with what was found for the analogous cationic X−TU complexes, in which unbridged Au···Au intermolecular separations of 3.2363(6)−3.3538(7) Å suggested extended aurophilic interactions, leading to a helical arrangement of Au(I) ions in the crystal for those systems. The absence of similar intermolecular Au···Au interactions for **1a**−**1d** may be the result of the more sterically demanding X−BIT ligands. The CF_3COO^- anion refines satisfactorily in **1a**−**1d**, but with large anisotropic thermal parameters, and is hydrogen bonded to the X−BIT ligands through the protonated and uncoordinated benzimidazole nitrogen atom, with N−H···O distances of ca. 2.7 Å (Table 2, Figure 5). The crystal structure for each cationic complex also reveals π stacking of one pair of the phenyl rings of the bridging dppm ligand with short interplanar distances of 3.39, 3.39, 3.46, and 3.49 Å for **1a**−**1d**, respectively, and angles between the ring planes ranging from 3.73(7) to 12.05(23)°, as shown for **1a** in Figure 6. In accordance with NMR spectroscopic data, the crystal structures reveal a disorder in the position of the X-substituent in **1b**−**1d** for two geometric isomers.

The neutral complexes **2a**, **2b**, and **2d** were also characterized crystallographically (Table 3), and show much different structural characteristics than their cationic counterparts. Whereas the coordination geometry around each Au(I) ion remains linear, the neutral dinuclear complexes actually crystallize as dimers, held together by an unbridged intermolecular distance that ranges between 2.8793(4) and 2.9822(8) Å. These separations are similar in magnitude to the intramolecular distances in the dinuclear complexes that span the values 2.8597(3)−2.9162(3) Å (for selected bond distances and angles see Table 4). These distances provide evidence of substantial aurophilicity and for the unsupported intermolecular separations are similar in strength to the intramolecular interactions in their cationic precursors. The intermolecular Au···Au distances in **2a**−**2b** and **2d** compare

Table 1. Cystallographic Data and Structure Refinement for **1a**−**1d**

	1a	1b	1c	1d
formula	$C_{34}H_{27}Au_2F_3N_2O_2P_2S{\cdot}CH_2Cl_2$	$C_{35}H_{29}Au_2F_3N_2O_2P_2S{\cdot}x$ Solvent	$C_{35}H_{29}Au_2F_3N_2O_3P_2S{\cdot}C_6H_{14}$	$C_{34}H_{26}Au_2ClF_3N_2O_2P_2S{\cdot}x$ Solvent
fw	1125.44	1054.55	1113.62	1074.75
T (K)	100.0(1)	193(2)	100.0(1)	100.0(1)
λ (Å)	0.71073	0.71073	0.71073	0.71073
cryst syst	monoclinic	monoclinic	monoclinic	monoclinic
space group	$C2/c$	$C2/c$	$C2/c$	$C2/c$
a (Å)	18.1091(7)	16.810(3)	16.4687(11)	16.793(3)
b (Å)	21.2668(8)	22.339(4)	21.6745(15)	22.211(4)
c (Å)	19.7968(7)	20.605(4)	21.3525(15)	20.428(4)
α (deg)	90	90	90	90
β (deg)	107.260(1)	102.613(3)	100.990(1)	103.059(3)
γ (deg)	90	90	90	90
V (Å^3)	7280.9(5)	7551(2)	7482.0(9)	7422(2)
Z	8	8	8	8
ρ_{calcd} (mg/m^3)	2.053	1.855	1.977	1.924
μ (mm^{-1})	8.393	7.950	8.030	8.159
cryst color	colorless block	colorless block	pale yellow-green block	colorless plate
cryst size (mm^3)	0.32 × 0.24 × 0.24	0.30 × 0.20 × 0.20	0.21 × 0.20 × 0.12	0.28 × 0.21 × 0.15
θ range (deg)	1.65−30.03	1.54−27.88	1.57−28.31	1.55−28.49
no. of data	10 575	8920	9271	9341
no. of params	458	425	501	434
GOF[a]	1.030	1.073	1.049	1.050
R1, wR2 (F^2, $I > 2\sigma(I)$)[b]	0.0199, 0.0457	0.0583, 0.1350	0.0338, 0.0929	0.0510, 0.1317
R1, wR2 (F^2, all data)[b]	0.0239, 0.0466	0.1023, 0.1457	0.0433, 0.0984	0.0773, 0.1416

[a] GOF = $S = [\sum w(F_o^2 - F_c^2)^2/(m - n)]^{1/2}$, where m = number of reflections and n = number of parameters. [b] R1 = $\sum||F_o| - |F_c||/\sum|F_o|$. wR2 = $[\sum w(F_o^2 - F_c^2)^2/\sum w(F_o^2)^2]^{1/2}$, where $w = 1/[\sigma^2(F_o)^2 + (aP) + bP]$ and $P = {}^1/_3 \max(0, F_o^2) + [2/3]\, F_c^2$.

Table 2. Selected Bond Lengths (Angstroms) and Angles (Degrees) for **1a**−**1d**

	1a	1b	1c	1d
Au···Au	2.90607(16)	2.8861(8)	2.8955(4)	2.8807(6)
Au−P, trans to N	2.2416(6)	2.245(3)	2.2376(14)	2.236(2)
Au−P, trans to S	2.2624(6)	2.264(3)	2.2636(13)	2.259(2)
Au−N	2.050(2)	2.073(8)	2.053(4)	2.070(7)
Au−S	2.3157(6)	2.319(3)	2.3138(13)	2.313(2)
N−H···OOCF$_3$	2.718(3)	2.700(13)	2.64(3)	2.691(10)
N−Au−P	179.07(6)	178.1(2)	177.85(15)	178.12(16)
S−Au−P	175.48(2)	176.51(9)	177.82(5)	176.85(7)
P−Au···Au (N)	93.192(16)	93.92(7)	92.61(4)	94.01(5)
P−Au···Au (S)	91.566(16)	90.30(7)	91.24(4)	90.25(6)
N−Au···Au	86.00(6)	84.9(2)	85.49(15)	85.54(19)
S−Au···Au	90.204(16)	91.08(8)	90.94(4)	91.09(6)

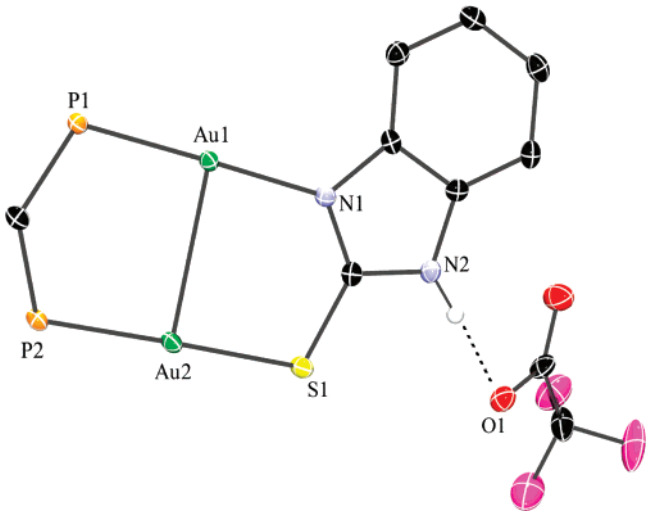

Figure 5. Perspective view of cationic **1a** interacting with CF_3COO^- anion; phenyl rings of dppm moiety omitted for clarity.

well with other unbridged Au···Au separations in neutral Au_2 complexes including 2.9235(4) Å in $[Au_2(\mu\text{-Me-TU})(\mu\text{-dppm})]_2{\cdot}3CH_3OH$[28] and 2.9617(7) Å in $[Au(S_2CN(C_5H_{11})_2)]_2{\cdot}DMSO$[37] and are in fact shorter than those found for the analogous complexes of $[Au_2(\mu\text{-NH}_2\text{-TU})(\mu\text{-dppm})]_2{\cdot}2CH_3OH{\cdot}H_2O$ and $[Au_2(\mu\text{-NH}_2\text{-TU})(\mu\text{-dppm})]_2{\cdot}8CH_3OH{\cdot}2H_2O$, which have intermolecular distances of 3.011 and 3.051 Å, respectively.[38] For **2a**−**b**, there are two unique half molecules per asymmetric unit, thus giving two independent intra- and intermolecular Au···Au distances (Table 4, Figure 7), whereas for **2d**, only one set of values for intra- and intermolecular Au···Au distances is obtained. The intermolecular aggregation in these neutral complexes might be due to the absence of the N−H imidazole proton, removing the possibility of hydrogen bonding with CF_3COO^- and/or polar solvent molecules. Whereas no additional Au···Au interactions beyond the dimer exist, it is important to note the short intermolecular distances within the dimers and the Au···Au···Au···Au configuration with dihedral angles spanning 105.12−140.12 ° in these complexes.

Absorption, Excitation, and Emission. The photophysical data for **1a**−**1d** and **2a**−**2d** are summarized in Tables 5−7. The solution absorption and emission data for **1a**−**1d** and **2a**−**2d** under steady-state conditions are shown in Figures 8 and 9, respectively. Both sets of complexes, **1** and **2**, exhibit intense ligand-centered absorptions at λ < 270 nm, whereas the near-UV transitions between 270 and 340 nm have molar absorptivities (ϵ) on the order of 10 000 dm^3 mol^{-1} cm^{-1}. These absorptions resemble those of the free X−BIT ligands, which are shown as Figure S7 in the Supporting Information. The higher-energy absorption maxima at ca. 279 nm are assigned to an intraligand transition of the bridging dppm moieties,[27] whereas the lower energy maxima at ca. 316 nm are tentatively assigned as a mixture of a

(37) Mansour, M. A.; Connick, W. B.; Lachicotte, R. J.; Gysling, H. J.; Eisenberg, R. *J. Am. Chem. Soc.* **1998**, *120*, 1329−1330.
(38) These structures were obtained by Young-A Lee and will be reported separately.

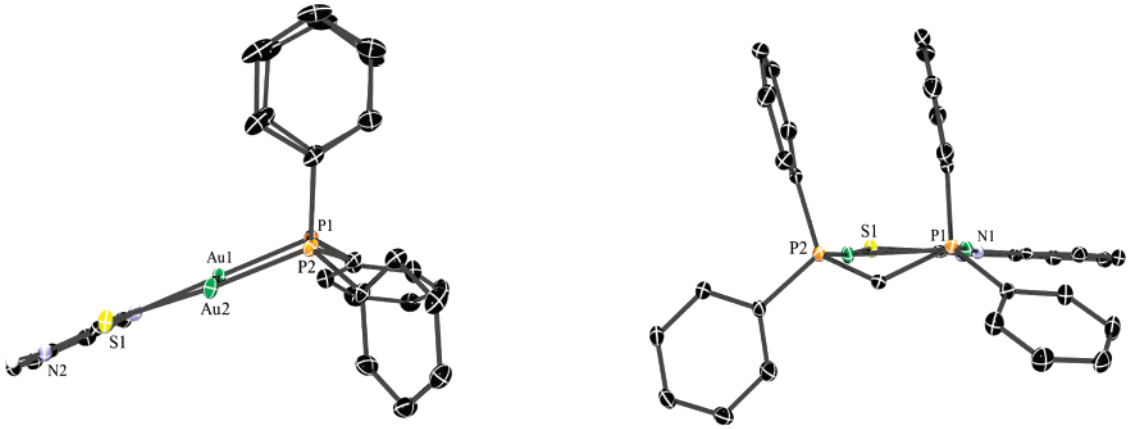

Figure 6. Perspective views of cationic **1a** showing π stacking in two of the phenyl rings of the bridging dppm ligand.

Table 3. Crystallographic Data and Structure Refinement for **2a**, **2b**, and **2d**

	2a	**2b**	**2d**
formula	$(C_{32}H_{26}Au_2N_2P_2S)_2 \cdot 2.5DMF$	$(C_{33}H_{28}Au_2N_2P_2S)_2 \cdot 4CH_3OH \cdot H_2O$	$(C_{32}H_{25}Au_2ClN_2P_2S)_2 \cdot x$ solvent
fw	2035.70	2027.20	1921.85
T (K)	100.0(1)	100.0(1)	100.0(1)
λ (Å)	0.71073	0.71073	0.71073
cryst syst	monoclinic	monoclinic	orthorhombic
space group	*C*2/*c*	*C*2/*c*	*Pccn*
a (Å)	32.4834(17)	34.066(6)	29.764(4)
b (Å)	17.0904(9)	17.125(3)	12.0886(17)
c (Å)	25.3173(13)	29.566(5)	17.881(3)
α (deg)	90	90	90
β (deg)	102.887(1)	124.571(2)	90
γ (deg)	90	90	90
V (Å^3)	13701.0(12)	14203(4)	6433.5(16)
Z	8	8	4
ρ_{calcd} (mg/m^3)	1.974	1.896	1.984
μ (mm^{-1})	8.746	8.437	9.382
cryst color	yellow needle	pale yellow plate	colorless needle
cryst size (mm^3)	0.38 × 0.05 × 0.05	0.38 × 0.16 × 0.04	0.38 × 0.06 × 0.01
θ range (deg)	1.29−30.51	1.39−30.51	1.37−28.28
no. of data	20 525	21 658	7980
no. of params	836	757	378
GOF[a]	1.062	1.056	1.066
R1, wR2 (F^2, $I > 2\sigma(I)$)[b]	0.0335, 0.0794	0.0596, 0.1312	0.0599, 0.1184
R1, wR2 (F^2, all data)[b]	0.0556, 0.0902	0.1433, 0.1725	0.1121, 0.1347

[a] GOF = $S = [\sum w(F_o^2 - F_c^2)^2/(m - n)]^{1/2}$, where m = number of reflections and n = number of parameters. [b] R1 = $\sum||F_o| - |F_c||/\sum|F_o|$. wR2 = $[\sum w(F_o^2 - F_c^2)^2/\sum w(F_o^2)^2]^{1/2}$, where $w = 1/[\sigma^2(F_o)^2 + (aP) + bP]$ and $P = {}^1/_3 \max(0, F_o^2) + [{}^2/_3] F_c^2$.

benzimidazolethiolate IL transition and an LMCT transition from the BIT thiolate donor to the Au(I) ion (S → Au).[18,39] For neutral complexes **2a**−**2d** in DMSO solution, similar absorption maxima are observed around 283 nm and 314 nm, corresponding to the same IL and IL/LMCT transitions as for the cationic complexes. For **2a**−**2d**, the lowest-energy absorption maxima corresponding to the mixed IL/LMCT transitions, decrease in the order X = H > Me ∼ OMe > Cl. For **1**, the analogous lowest-energy absorption maxima decrease in the order X = H > Me > Cl > OMe.

The emission spectra for **1a**−**1d** in CH_2Cl_2 solution (Figure 8) differ from those of the corresponding free X−BIT ligands in CH_3OH/CH_2Cl_2 solution (Figure S8 in the Supporting Information). The emission maxima for **1a**−**1d** lie in the UV region at ca. 365 nm, with **1c** having an additional maximum at 465 nm. The lower energy emission maximum for **1c** is highly concentration dependent. While absent at a concentration of 10^{-7} M, the emission increases relative to that at 364 nm, reaching a maximum ratio at 10^{-4} M. At an even higher concentration of 10^{-3} M, the emission at 465 nm is no longer observed, possibly as a consequence of self-quenching (Figure S9 in the Supporting Information). Room-temperature excitation spectra of **1c** with $\lambda_{em} = 370$ nm and 470 nm show no exceptional difference (Figure S10 in the Supporting Information). The λ_{em}^{max} of complexes **1** do not show a significant change on going from **1a** to **1d**, an indication that the emission is either purely ligand-based (in which case the X substituent affects the HOMO and LUMO energies in similar ways) or MC.

Contrary to the cationic complexes, the emission spectra for the neutral series **2** in DMSO solution (Figure 9) show that λ_{em}^{max} changes substantially on going from **2a**−**2d**. The change in λ_{em}^{max} clearly indicates the involvement of the X−BIT ligand in the excited-state. Considering the absence of this characteristic shift in cationic series **1**, the assignment

(39) Narayanaswamy, R.; Young, M. A.; Parkhurst, E.; Ouellette, M.; Kerr, M. E.; Ho, D. M.; Elder, R. C.; Bruce, A. E.; Bruce, M. R. M. *Inorg. Chem.* **1993**, *32*, 2506−2517.

Table 4. Selected Bond Lengths (Angstroms) and Angles (Degrees) for **2a**, **2b**, and **2d**[a]

	2a		**2b**		**2d**[b]
intra Au···Au	2.8597(3)	2.9162(3)	2.8930(7)	2.8984(7)	2.9080(6)
inter Au···Au	2.8793(4)	2.9457(4)	2.9019(8)	2.9457(9)	2.9822(8)
Au−P, trans to N	2.2281(13)	2.2471(13)	2.246(3)	2.244(3)	2.235(3)
Au−P, trans to S	2.2827(12)	2.2728(12)	2.277(3)	2.270(3)	2.266(3)
Au−N	2.023(4)	2.047(4)	2.066(10)	2.058(9)	2.15[b]
Au−S	2.3237(12)	2.3151(12)	2.302(3)	2.303(3)	2.34[b]
		Intramolecular			
N−Au−P	175.70(13)	178.75(11)	178.3(3)	178.3(3)	176[b]
S−Au−P	176.88(4)	178.17(5)	176.26(14)	175.23(12)	175.3[b]
P−Au···Au (N)	95.88(3)	93.56(3)	93.07(8)	93.53(7)	92.54(7)
P−Au···Au (S)	88.17(3)	90.44(3)	91.86(7)	90.85(7)	91.86(7)
N−Au···Au	86.13(11)	86.49(11)	87.6(3)	87.4(3)	87[b]
S−Au···Au	89.93(3)	89.46(3)	89.36(8)	89.24(9)	88.7[b]
		Intermolecular			
P−Au···Au (S)	94.75(3)	94.78(3)	96.85(8)	95.89(7)	101.15(7)
S−Au···Au	87.94(3)	86.16(3)	84.17(8)	86.61(9)	81.2[b]
Au···Au···Au	158.085(9)	152.014(9)	144.36(3)	146.83(3)	136.60(3)
Au···Au···Au···Au	105.12	114.20	122.95	116.54	140.12

[a] For complexes **2a** and **2b**, there were two unique half-molecules per asymmetric unit; for **2d**, only one unique half-molecule per asymmetric unit. [b] **2d** showed severe disorder, and therefore these parameters are taken as the averages of a modeled disorder (CIF for more information).

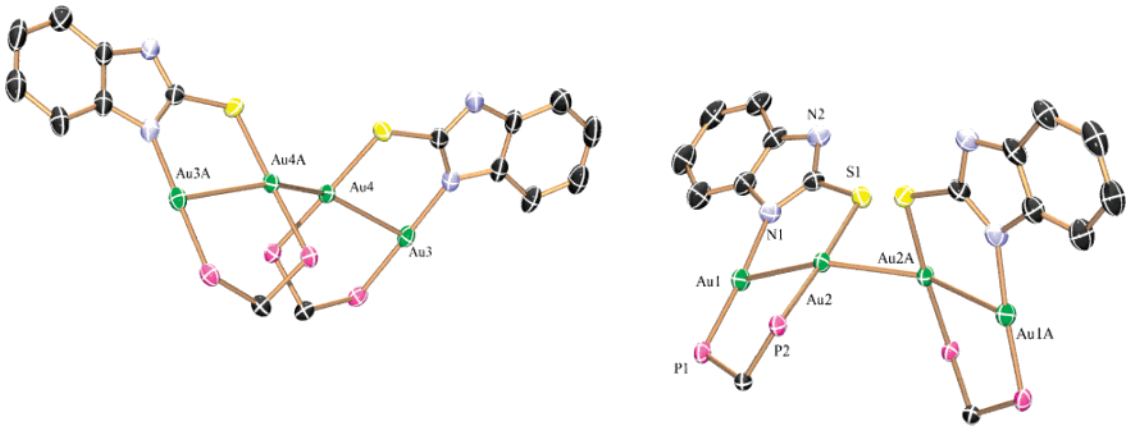

Figure 7. Perspective view of the two unique dimers of neutral **2a**, having intra and intermolecular Au···Au interactions; phenyl rings of the dppm moiety were omitted for clarity.

Table 5. Photophysical Data for **1a**−**1d**

	λ_{abs}/nm (ϵ/dm^3 mol^{-1} cm^{-1})[a]	soln λ_{em}/nm[a,b]	solid-state λ_{em}^{max}/nm[c]
1a	278 (21 400), 310 (9100)	355 (sh), 364 (max), 380 (sh)	469
1b	280 (21 760), 314 (9790)	355 (sh), 364 (max), 380 (sh)	472
1c	280 (25 890), 322 (10 350)	355 (sh), 364 (max), 380 (sh), 465	476
1d	279 (22 430), 317 (14 320)	355 (sh), 365 (max), 380 (sh)	475

[a] 1.0×10^{-5} M in CH_2Cl_2. [b] λ_{ex} = 320 nm. [c] 10% (w/w) mixture with KBr, λ_{ex} = 395 nm.

Table 6. Photophysical Data for **2a**−**2d**

	λ_{abs}/nm (ϵ/dm^3 mol^{-1} cm^{-1})[a]	soln λ_{em}^{max}/nm[a,b]	solid-state λ_{em}^{max}/nm[c]
2a	281 sh (25 720), 312 sh (14 450)	499	523
2b	284 sh (18 720), 313 sh (10 840)	514	534
2c	285 sh (26 330), 313 sh (11 760)	543	533
2d	283 sh (29 340), 316 sh (13 860)	486	512

[a] 1.0×10^{-5} M in DMSO. [b] λ_{ex} = 290 nm. [c] 10% (w/w) mixture with KBr, λ_{ex} = 440 nm.

Table 7. Luminescence Tribochromism Data for **1a**, **1b**, and **1d**

	solid-state crystals λ_{em}^{max}/nm[a]	solid-state crushed λ_{em}^{max}/nm[b]	ΔE/cm^{-1} [c]
1a	484	459	1130
1b	481	466	670
1d	478	459	870

[a] λ_{ex} = 365 nm. [b] Measured as a solid-state mixture with KBr, λ_{ex} = 365 nm. [c] $\Delta E = E_{crushed} - E_{crystals}$.

for the emission of the neutral series **2** is most likely that of an LMMCT, due in part to the extended Au···Au interactions.[4,40] We can also correlate the emission energies of **2** with Hammett constant values for the substituent X in either the para- (σ_p) or meta- (σ_m) position[41] relative to the Au−N imidazole nitrogen on the ligands (Scheme 3). For σ_p Hammett constant values, the data correlate very well; the most electron-donating OMe−BIT ligand (**2c**) has the lowest λ_{em}^{max}, whereas **2d** has the highest λ_{em}^{max} due to the more

(40) Yam, V. W.-W.; Lo, K. K.-W. *Chem. Soc. Rev.* **1999**, *28 (5)*, 323−334.

(41) Smith, M. B.; March, J. *March's Advanced Organic Chemistry: Reactions, Mechanisms, and Structure*, 5th Ed.; 2000; p 1824.

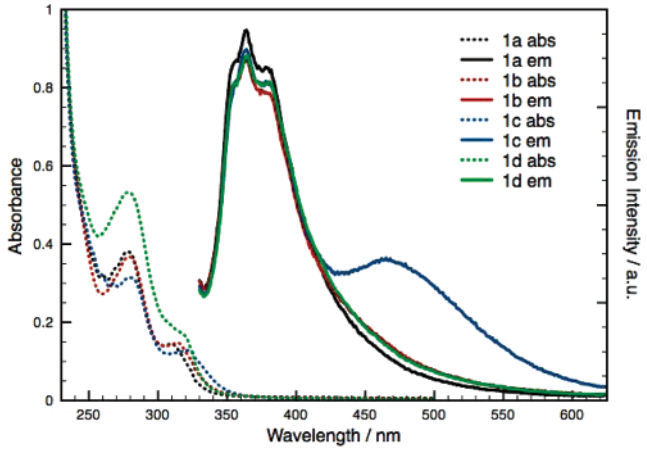

Figure 8. Room-temperature absorption and emission (λ_{ex} = 320 nm) spectra for **1a**−**1d** in 1.0 × 10^{-5} M CH_2Cl_2 solution.

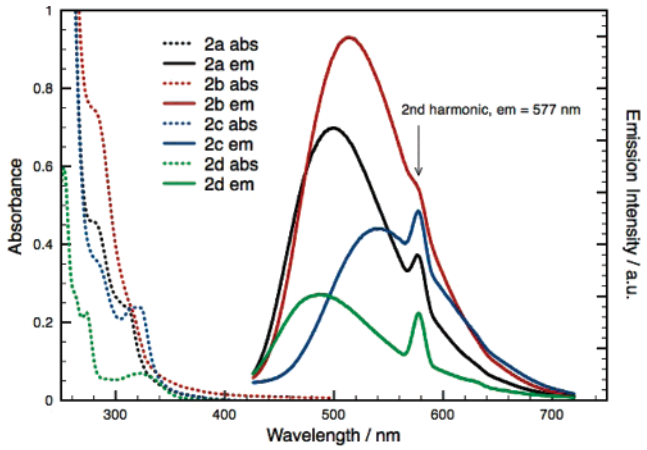

Figure 9. Room temperature absorption and emission (λ_{ex} = 290 nm) spectra for **2a**−**2d** in 1.0 × 10^{-5} M DMSO solution.

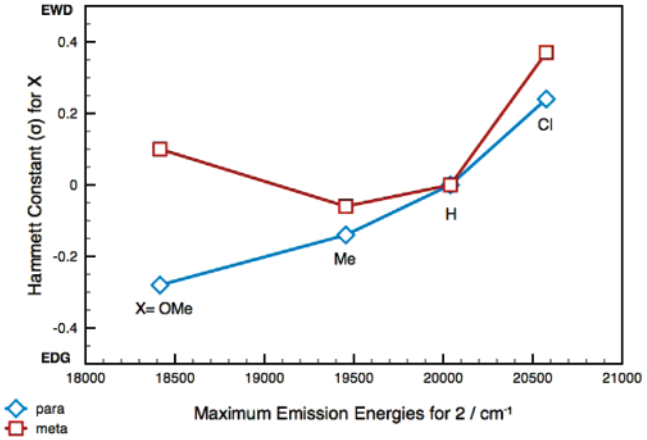

Figure 10. Correlation between σ_p and σ_m Hammett constants[41] versus emission energy for **2a**−**2d** in 1.0 × 10^{-5} M DMSO solution.

electron-withdrawing Cl−BIT ligand (Figure 10). The σ_m Hammett constants for **2a**, **2b**, and **2d** also correlate in a similar fashion with the emission energies, but the correlation does not hold for the −OMe substituent.

When comparing the λ_{em}^{max} for solution emission spectra between the cationic series **1** and the neutral series **2**, there is a significant shift from higher to lower energy, respectively. This shift may result from either or both of the

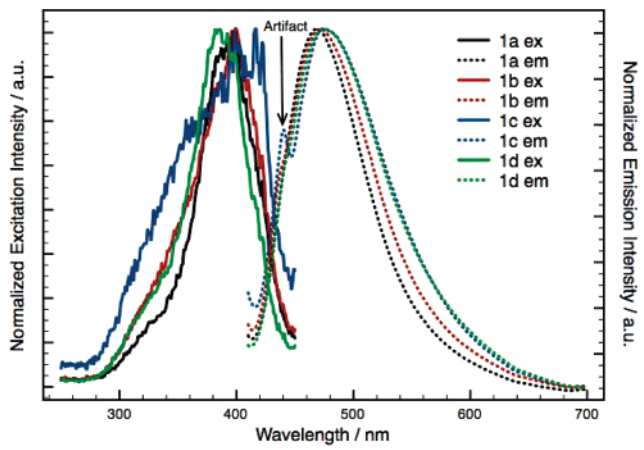

Figure 11. Solid-state excitation (λ_{em} = 465 nm) and emission (λ_{ex} = 395 nm) spectra for **1a**−**1d** in a 10% (w/w) mixture with KBr at room temperature.

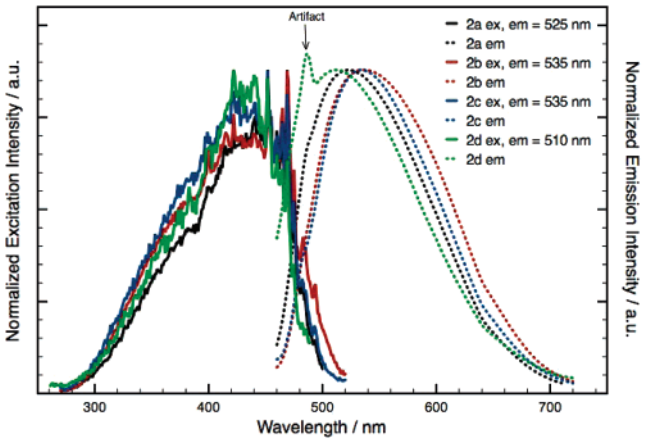

Figure 12. Solid-state excitation and emission (λ_{ex} = 440 nm) spectra for **2a**−**2d** in a 10% (w/w) mixture with KBr at room temperature.

following effects: (1) configuration mixing due in part to the extended Au···Au···Au···Au intermolecular interactions found in the structures of the neutral complexes,[40,42] a property not observed for the cations; and (2) change in the overall charge of the complex, from monocationic to neutral.

The solid-state emission spectra of **1** and **2** were done in a matrix of KBr at room temperature and are summarized in Tables 5−7. For the series of cationic complexes **1**, the excitation spectra mirror the emission spectra, with emission maxima of 469, 472, 476, and 475 nm for **1a**−**1d**, respectively, when λ_{ex} = 395 nm (Figure 11). Like the emission spectra in the CH_2Cl_2 solution, the small change in λ_{em}^{max} in the solid-state indicates the X−BIT ligands are having little to no effect on the excited-state of the complexes, indicating that the emission is either ligand-based or MC in nature.

Like their cationic counterparts, the excitation spectra of **2a**−**2d** mirror their respective emission spectra, but the corresponding solid-state emission spectra of the neutral complexes **2a**−**2d** show red-shifted maxima of 523, 534, 533, and 512, respectively, when λ_{ex} = 440 nm (Figure 12). As in DMSO solution, the solid-state emission spectra of

(42) Balch, A. L. *Gold Bulletin* **2004**, *37 (1−2)*, 45−50.

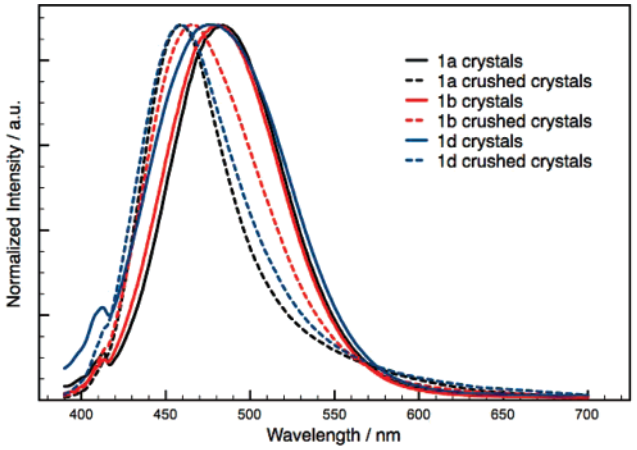

Figure 13. Solid-state emission (λ_{ex} = 365 nm) spectra showing luminescence tribochromism of **1a**−**1b** and **1d** in a finely ground matrix of KBr at room temperature.

2a−**2d** show a correlation between λ_{em}^{max} and the X substituent of X−BIT. The energies for λ_{em}^{max} increase in the order X = Cl > H > OMe ≈ Me, a trend that follows well with having a mixture of *m*- and *p*-isomers in the solid-state samples. The excited-state transitions for solid samples of **2a**−**2d** are comparable to those in DMSO solution and are tentatively assigned as LMMCT in nature. In fact, the lifetime for a solid-state sample of **2c** was measured to be 0.2 μs when λ_{ex} = 400 nm. Ma and Che reported similar lifetime measurements for the dinuclear Au(I) complex, [Au_2(dppm)Cl_2], which had triplet excited lifetimes of 0.15, 0.3, and 0.45 μs in CH_3CN solution, solid-state, and in the poly(methyl methacrylate) (PMMA) matrix, respectively.[5]

Luminescence Tribochromism. A unique solid-state emission property that is observed with **1a**, **1b**, and **1d** is that of luminescence tribochromism.[43,44] When X-ray quality crystals of **1a**, **1b**, and **1d** are irradiated with 365 nm light, they show emission maxima of 484, 481, and 478 nm, respectively (Figure 13). Upon gentle crushing of the crystals with a spatula, the emission maxima shift to higher energies: 459, 466, and 459 for **1a**, **1b**, and **1d**, respectively; a change in emission energies that ranges from 670 to 1130 cm^{-1} (Table 7). For **1c**, this unique mechanical effect is not observed to the extent of the other three cationic complexes; the change in emission upon grinding crystals of **1c** is within the error of the instrument.

Lee and Eisenberg previously reported a similar luminescence phenomenon for the analogous cationic [Au_2(μ-X−TU)(μ-dppm)]Y complexes, where X = H, Me, and Y^- = NO_3^-, ClO_4^-, and $Au(CN)_2^-$.[28] In their study, solid samples of the cationic complexes were either nonemissive or weakly photoluminescent, and after gentle crushing the solid samples exhibited bright blue or cyan photoluminescence. The effect was attributed in part to (1) disruption of weak Au···Au intermolecular interactions accompanied by rearrangement to dimers having stronger intermolecular contacts; and (2) the evolution of volatile acid upon crushing. A somewhat similar behavior was described by Assefa et al., who reported that the 1D chain compound, [$(TPA)_2Au$][$Au(CN)_2$] (TPA = 1,3,5-triaza-7-phosphaadamantane), that was not luminescent in the visible region in crystalline form, became brightly emissive when ground to a fine powder.[45] However, these authors proposed a different basis for the observation in terms of localized lattice defects in the emissive powder that encompass dimeric or oligomeric units. Both reports differ from the present study in that solid samples of the cationic complexes **1a**, **1b**, and **1d** reported here are green emissive *prior* to crushing, shifting to higher energy after grinding.

In contrast with the earlier report involving [Au_2(μ-X−TU)(μ-dppm)]Y complexes,[28] the cationic complexes **1a**, **1b**, and **1d** exhibit no evolution of volatile CF_3CO_2H after gentle heating or sonication. Furthermore, there is no correlation between the solid-state emission maxima of the crushed form of **1a**, **1b**, and **1d** and those of the neutral complexes **2a**, **2b**, and **2d**, which is in contrast with what *was* observed for the cationic and neutral [Au_2(μ-X−TU)(μ-dppm)]$^{+/0}$ complexes.

The origin of the luminescence tribochromism observed in the present study thus differs from the earlier reports.[28,45] One difference may lie in the bulkiness of the X−BIT ligands that prevents extended or chainlike intermolecular Au···Au interactions from occurring in the cationic complexes, **1a**−**1d**, which is not the case for the dinuclear cations bridged by the less-bulky X−TU ligands in Lee's study. At this point, the basis of luminescence tribochromism in the complexes described here, as well as in the previously reported systems, can only be conjectured and will require unambiguous assignments of the emissive states in these complexes. Additional photophysical studies will be required, including lifetime measurements and an analysis of systematic substituent effects on photophysical properties to accomplish this goal.

Conclusions

We have successfully synthesized a series of new cationic and analogous neutral dinuclear Au(I) phosphine thiolate complexes that exhibit interesting structural and luminescence properties that include short intramolecular Au···Au interactions, with no extended aggregation observed and luminescence tribochromism that occurs upon mechanical grinding of microcrystalline samples of the cationic systems to powder. The neutral complexes crystallize as dimers with significant intra- and intermolecular Au···Au interactions, which causes the λ_{em}^{max} to shift substantially to the red region when compared to the emission maxima of the cations. Both sets of complexes possess a wide variety of structural and photophysical properties that lead to excited-state assignments that include LMCT, ligand-based, MC, and LMMCT states.

Acknowledgment. We thank the Eastman Kodak Company, the National Science Foundation (Grant CHE-

(43) Asiri, A. M. A.; Heller, H. G.; Hursthouse, M. B.; Karalulov, A., *Chem. Commun.* **2000**, 799−800.
(44) Bouas-Laurent, H.; Durr, H. *Pure Appl. Chem.* **2001**, *73*, 639−665.
(45) Assefa, Z.; Omary, M. A.; McBurnett, B. G.; Mohamed, A. A.; Patterson, H. H.; Staples, R. J.; Fackler, J. P., Jr. *Inorg. Chem.* **2002**, *41*, 6274−6280.

0207018), and the donors of the Petroleum Research Fund administered by the American Chemical Society (Grant PRF # 36243-AC3) for support of this research. We also thank Mr. Terry O'Connell for assisting with mass spectrometric measurements and Dr. Paul Merkel for help with the lifetime measurement of **2c**.

Supporting Information Available: Perspective views of **1a** showing phenyl π stacking, cationic complexes **1b**−**1d** interacting with CF_3COO^- anion and dimers of **2b** and **2d**, room temperature absorption and emission spectra of free X−BIT ligands, room-temperature emission spectra of **1c** at varying concentrations, and room-temperature excitation spectrum of **1c**. Crystallographic data is in CIF format. This material is available free of charge via the Internet at http://pubs.acs.org.

IC701763X